Eur. Phys. J. B **35**, 209–216 (2003)
DOI: 10.1140/epjb/e2003-00270-8

THE EUROPEAN PHYSICAL JOURNAL B

Far-infrared probe of size dispersion and population fluctuations in doped self-assembled quantum dots

J.N. Isaia[1], L.A. de Vaulchier[1,a], S. Hameau[1], R. Ferreira[1], Y. Guldner[1], E. Deleporte[1,b], J. Zeman[2], V. Thierry-Mieg[3], and J.M. Gérard[3,c]

[1] Laboratoire de Physique de la Matière Condensée, École Normale Supérieure, 24 rue Lhomond, 75231 Paris Cedex 05, France
[2] Grenoble High Magnetic Field Laboratory, CNRS/MPI, 25 avenue des Martyrs, 38042 Grenoble Cedex 9, France
[3] Laboratoire de Photonique et Nanostructures, Route de Nozay, 91460 Marcoussis, France

Received 7 May 2003 / Received in final form 22 July 2003
Published online 2 October 2003 –

Abstract. We investigate the FIR magneto-optical transitions in doped self-assembled InAs quantum dots with an average filling ranging from 0.6 to 6 electrons per dot. Significant changes in the magnetic field dispersion, the line-width and the amplitude of the transitions are observed as the doping level is varied, in agreement with our theoretical calculations. We show that our technique is an effective tool to obtain informations regarding the dot size homogeneity and the electron filling uniformity.

PACS. 73.21.La Quantum dots – 78.20.Ls Magnetooptical effects – 78.30.Fs III-V and II-VI semiconductors – 78.67.Hc Quantum dots

1 Introduction

Doped self-assembled InAs/GaAs quantum dots (QD) open new perspectives both in fundamental physics (for instance the strong coupling regime between electrons and optical phonons [1–3]) and for device applications (for instance QD far-infrared photodetectors [4–8] or solid-state qubits for quantum computing [9,10]). For basic physics and for device design, it is crucial to obtain information regarding the QD electron filling uniformity. Spatial variations of the QD filling can originate from various effects: composition fluctuations, statistical distribution of the dopants, size dispersion of the QD. The far-infrared (FIR) magneto-absorption technique is an effective tool to investigate the electronic excitations in QD [1,3,11]. Previous theoretical calculations predicted that FIR magneto-absorption spectra should depend significantly on the QD filling [12] and FIR spectroscopy was used to study the electronic excitation as a function of the QD filling [13]. But to date, there was no investigation of the influence of the QD filling fluctuations on the FIR magneto-spectra. We report here an investigation of the far-infrared (FIR) magneto-optical transitions up to $B = 28\,\text{teslas}$ at $T = 2\,\text{K}$ in samples with increasing doping levels in order to transfer, on average, $N = 0.6$ to 6 electrons per dot and to populate the s and p states (states with an angular momentum projection along the growth axis $L_z = 0, \pm\hbar$). Significant changes in the dispersion, the line-width and the amplitude of the FIR transitions are observed as the doping level is varied. The energy positions of the observed resonances are consistent with our theoretical calculations of the electronic levels. Using a realistic QD shape, we predict that up to six electrons can be confined at low temperature. Nevertheless the experiments evidence a delocalization of some electrons in the wetting layer for a filling $N = 6$. We also show that the resonance lineshape can be accounted by the filling fluctuations resulting from the QD size dispersion. The QD size distribution is evaluated from the analysis of the FIR magnetotransmission and PL results measured on the samples with lowest doping levels. We then evaluate the resulting fluctuations of the QD filling for each sample. Finally, we simulate the lineshape of the resonances observed in samples with various doping. The simulation reproduce rather well the intensities and lineshape of the experimental resonances. We also evaluate the line broadening arising from the statistical distribution of the dopants and we conclude that the size dispersion constitutes the dominant effect which governs the filling uniformity in our samples.

[a] e-mail: Louis-Anne.deVaulchier@lpmc.ens.fr
[b] *Present address:* Laboratoire de Photonique Quantique et Moleculaire, École Normale Superieure de Cachan, 94235 Cachan Cedex, France
[c] *Present address:* CEA-Grenoble DRFMC/SP2M/PSC, Laboratoire de Physique des semiconducteurs, 38054 Grenoble, France

Table 1. Doping and average QD electron filling for the six samples An and Bn ($n = 1, 2, 3$).

Sample	doping ($\times 10^{10}$ cm^{-2})	average QD electron filling (e/dot)
A1	3.5	0.6
A2	13	3
A3	11	2.5
B1	9	2
B2	17	4
B3	25	6

2 Samples

Two series of samples, labelled An and Bn ($n = 1, 2, 3$), have been grown by MBE. In each series the doping level was varied from sample to sample, all the other growth parameters being exactly similar. Each sample contained a multistack of 20 layers of InAs QDs separated by 50 nm GaAs barriers, each layer having a QD density of 4×10^{10} cm^{-2}. The InAs QD were formed by depositing 2.2 monolayers (MLs) at 520 °C with a growth rate of 0.11 ML/s. There was no growth interruption before GaAs overgrowth. Details about the growth procedure are given elsewhere [14,15]. The QD electron filling was realized by a Si δ-doping of the GaAs barriers at 2 nm under the dot layer. The δ doping concentration ranged between 3.5×10^{10} and 25×10^{10} cm^{-2} in order to get a QD filling from 1 to 6 electrons. This is reported for all our samples in Table 1.

The doping level was calibrated by performing Hall measurements on thick doped GaAs layers. We checked that the average QD filling, estimated from the integrated intensity of the FIR absorption lines as described in Appendix A of reference [3], was in agreement with the MBE calibrations. The emission peak energy, given by PL experiments at liquid helium temperature, was in the range 1.15−1.20 eV. Cross-sectional transmission electron spectroscopy [15] or cross-sectional scanning tunnelling microscopy [16] in samples grown in similar conditions have shown that the QDs resemble flat truncated cones with a $\sim$ 20 nm basis diameter and a height ranging between 2 and 4 nm.

3 Experimental results

We have investigated the FIR magneto-optical transitions between the ground and the first excited conduction-band states. The sample transmission at 2 K was recorded by Fourier-transform spectroscopy in the FIR range 20–100 meV for magnetic field up to $B = 28$ T. For each sample, the transmission was normalized to that of the substrate in order to eliminate the optical setup effects. Figure 1 shows the transmission spectra recorded at $B = 8$ and 15 teslas on samples A1, A2 and A3. As

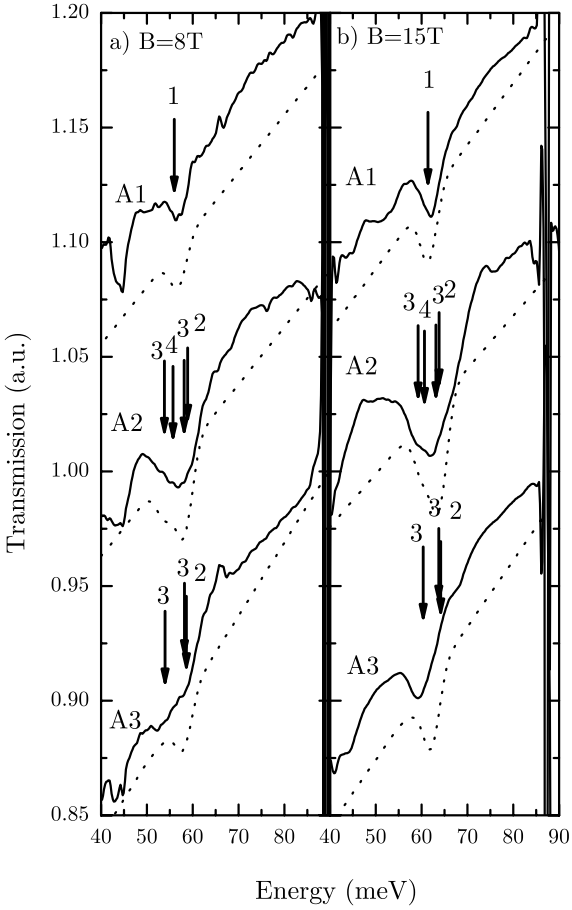

Fig. 1. Infrared transmission spectra at (a) $B = 8$ teslas and (b) $B = 15$ teslas at $T = 2$ K of samples labelled A1, A2 and A3. The arrows with the label N ($N = 1, ..., 4$) indicate the calculated position of the magneto-optical transitions for QDs with electron filling N. The dotted lines are the simulated spectra as described in Section 5.

the An samples correspond to the same series, all the growth parameters are exactly similar except the doping level of the GaAs barriers which is 3.5×10^{10}, 13×10^{10} and 11×10^{10} cm^{-2} respectively. Considering the p-type residual doping ($\sim 2 \times 10^{15}$ cm^{-3}) of the 50 nm thick GaAs barriers, the electron density available for transferring into a QD plane is 2.5×10^{10}, 12×10^{10} and 10×10^{10} cm^{-2} respectively, corresponding to an average QD electron filling of 0.6 (A1), 3 (A2) and 2.5 (A3).

At $B = 8$ T, two pronounced transmission minima are observed for each sample. The energy of the higher minimum (at $\sim$ 57 meV) goes up when B is increased while the opposite dependence is observed for the lower minimum at $\sim$ 44 meV. This behavior arises from the orbital Zeeman effect of the p states as described below. Finally, at $B = 15$ T, only the higher minimum is observed at $\sim$ 60 meV, the lower minimum being shifted by the magnetic field into the restrahlen band of the GaAs substrate ($30 - 40$ meV). The transmission minima in A1 are surprisingly sharp with a fullwidth at half maximum (FWHM) of $\sim$ 3 meV, while the minima in A2 are obviously much broader with a FWHM of $8 - 10$ meV. Finally,

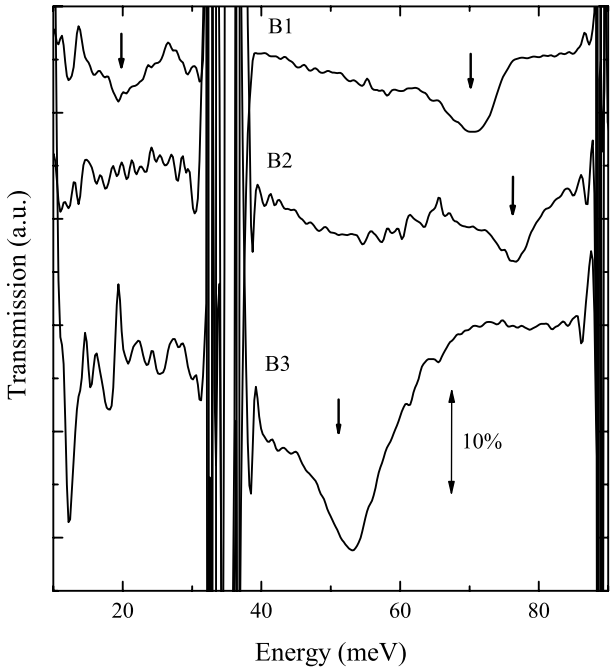

Fig. 2. Infrared transmission spectra at $B = 28$ teslas in samples B1, B2 and B3, whose average QD fillings are 2, 4 and 6 respectively. The arrows indicate the minimum of transmission.

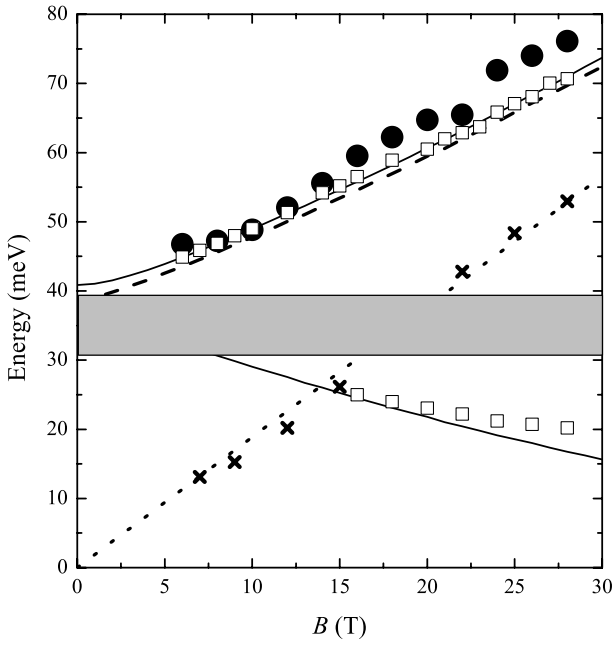

Fig. 3. Magnetic field dispersion of the transmission minima for the three samples B1 (open squares), B2 (full dots) and B3 (crosses), and theoretical calculations (B1: solid lines, B2: dashed line and B3: dotted line). The grey rectangle shows the absorption zone due to the substrate restrahlen.

it is clear in Figure 1 that both the amplitude and the line-width of the FIR transitions depend significantly on the doping level.

Figure 2 displays FIR spectra recorded at $B = 28$ T on samples B1, B2 and B3. In the series Bn, the doping level was adjusted in order to get an average filling of 2 (B1), 4 (B2) and 6 (B3) taking into account the p-type residual doping of the barrier. The spectra are clearly drastically dependent on the doping level. Sample B1 displays two minima indicated by the arrows while B2 presents only a high energy resonance. The absorption in both samples have an amplitude of 5–6% with a FWHM of ~ 7 meV. Different results are observed in sample B3 where a single intense and broad minimum is observed at a lower energy than in B1 and B2 with an amplitude $> 15\,\%$ and a FWHM > 10 meV. The B-dispersion of the transmission minima are shown in Figure 3. Samples B1 and B2 exhibit a QD behavior with transitions extrapolating at $B = 0$ to an energy of ~ 35 meV. On the contrary, the resonance energy in sample B3 extrapolates to zero at $B = 0$ which does not correspond with a QD excitation but is the behavior expected for a cyclotron resonance (CR) in a two dimensional electron gas (2DEG).

We have also done PL measurements at 2 K on the different samples. The PL peak obtained for a non-resonant excitation in the wetting layer is rather broad with a FWHM of $\sim 80 - 100$ meV as illustrated in Figure 4 for samples B1 and A3.

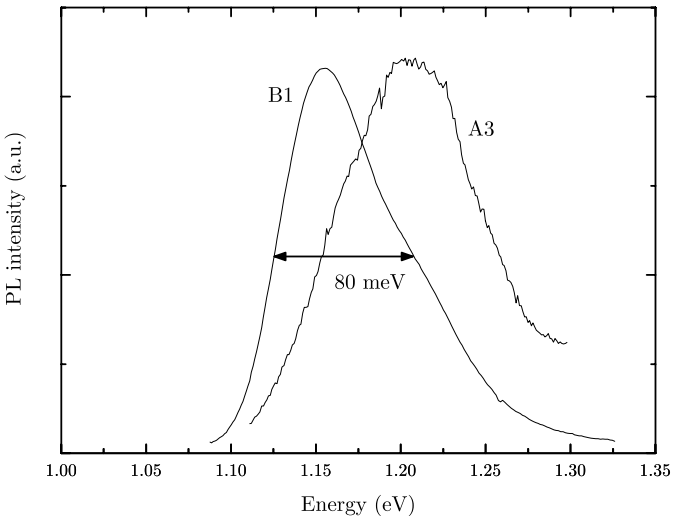

Fig. 4. Photoluminescence spectra of samples B1 and A3 at zero magnetic field with an energy excitation of 1.45 eV at low power excitation.

4 Theoretical aspects

In order to analyse the previous experimental results, we have calculated the few-electron states of a QD under magnetic field. We have used a realistic QD shape and confining potential unlike previous calculations using the Fock-Darwin states of an infinite parabolic potential [12]. The QDs are modelled by a truncated cone of height $h \sim 2$ nm and basis angle 30°. An elliptical dot basis is assumed with minor and major axes a and b around 10 nm to

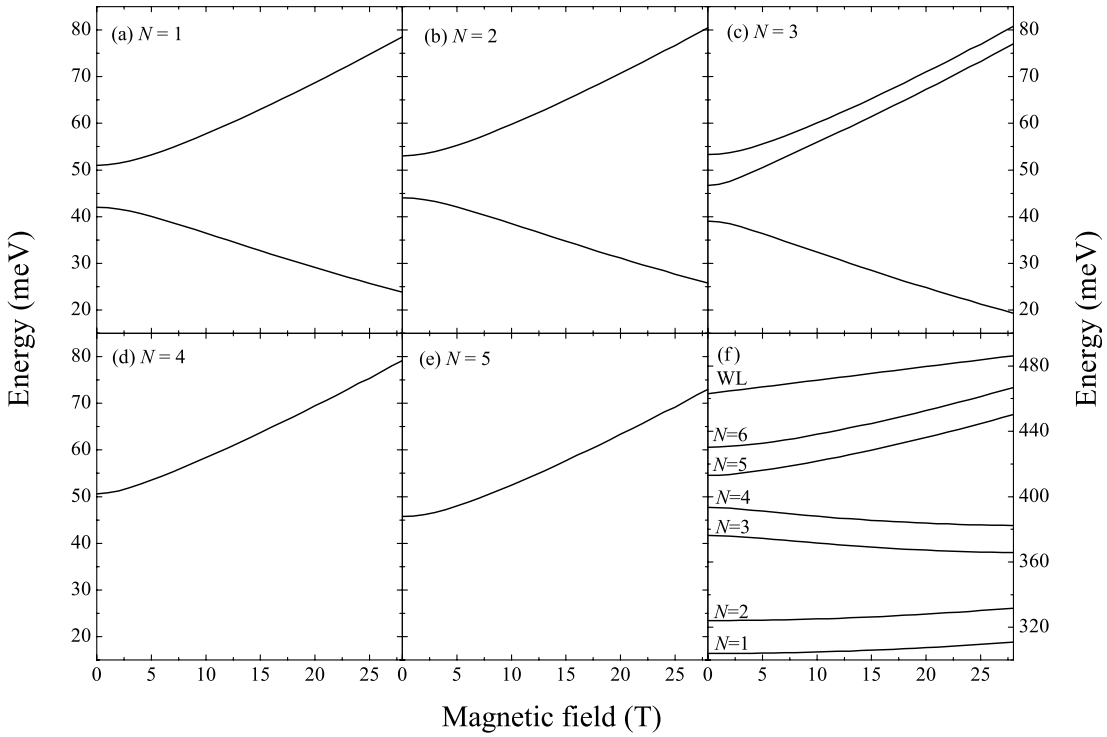

Fig. 5. (a) to (e): solid lines: predicted magneto-optical transitions for $N = 1$ to 5, using QD parameters given in the text. (f): QD chemical potential for $N = 1$ to 6 electrons and energy edge of the wetting layer.

account for the slight QD elongation which is experimentally observed [3] along the in-plane direction [1,−1,0] as compared to the [1,1,0] one. In order to include the intermixing effects between the InAs layers and the GaAs barriers, we have considered an homogeneous gallium content of 30 % in the QDs. The conduction (valence) band discontinuity between InGaAs and GaAs is then 488 meV (217 meV) and the confining potential taking into account the wetting layer (WL) is 460 meV (201 meV) if one considers a WL thickness of 1 monolayer (ML) and the following effective masses: $m^* = 0.06m_0$ for the conduction band, $m^*_{h_z} = 0.30m_0$ and $m^*_{h_{xy}} = 0.10m_0$ for the heavy hole states. The single-electron states are calculated using a variational procedure with Gaussian functions [17]. For QDs containing N electrons ($N \leq 6$), the basis of the few-electron Hilbert space is constructed from the antisymmetrized product of single electron s and p states ($L_z = 0, \pm\hbar$) [18]. Neither the d states ($L_z = \pm 2\hbar$), nor the mixing with the continuum of the wetting layer and GaAs barriers, are included in the model. The validity of such approximations will be discussed below. The diagonalization of the N-electron Hamiltonian including the Coulomb terms, leads to the determination of the ground and first excited states as a function of the magnetic field. The energy and the oscillator strength of the FIR magneto-optical transitions are then calculated in the electric dipole approximation. The solid lines in Figures 5a to e show the predicted FIR magneto-optical transitions for $N = 1$ to 5 respectively, using $h = 2.6$ nm, $a = 11.9$ nm, $b = 13.1$ nm. These are best-fit parameters for the FIR experimental results obtained on sample A1. Only transitions with oscillator strength larger than 5% are displayed. The electron-phonon interaction and the so-called polaron effects [1,3] are not included in these calculations. The transition energy either increases or decreases as a function of B, arising from the orbital Zeeman effect of the p states. Note that the magneto-optical transitions are found depending on N, which was expected as the confining potential is not purely parabolic [12]. The chemical potential of N electrons in a QD is defined by $\mu_N = E_{\text{ground}}(N) - E_{\text{ground}}(N-1)$ where $E_{\text{ground}}(N)$ is the energy of the ground state of the N electrons in the QD. It is the energy cost of introducing the Nth electron in the QD. μ_1 represents the energy of a single electron in a QD (ground state). Figure 5f shows the chemical potential for $N = 1$ to 6 (*i.e.* the energy cost of introducing one more electron in a QD) as well as the energy edge of the WL. For these parameters, up to 6 electrons can be transferred into the QDs with energy below the WL.

Note that, at $B = 0$, $\Delta\mu = \mu_{N+1} - \mu_N$ is typically ~ 20 meV except for $N = 2$ which corresponds to the filling of the s shell. $\Delta\mu$ is then ~ 50 meV. At $B \neq 0$, we also calculate $\Delta\mu \sim 20$ meV except for $N = 2$ and for $N = 4$ which corresponds to the filling of the p^- states ($L_z = +\hbar$). For $N = 4$, $\Delta\mu$ is found to strongly increase with B because of the orbital Zeeman effect and reaches ~ 70 meV at $B = 28$ T.

5 Analysis of the experimental results

As shown in Section 3, the line-width of the FIR magneto-optical transitions is found to be strongly depending on

the doping level of the samples and thus on the QD electron filling. Different effects can be invoked to explain the observed widths, mainly the distribution of ionized dopants and the size dispersion of the QD.

Let us first evaluate the perturbation of the dot levels by the ionized dopants. This perturbation decomposes into two contributions: an average (band-bending) field, due to a uniform distribution of impurities, plus fluctuations due to the statistical distribution in the doping plane. The bound states are strongly confined in the dot and have rather similar distribution probabilities along the growth axis. As a consequence, the average field equally affects the bound levels. In addition, it is unable to directly couple dot levels of different in-plane symmetries. One can thus readily convince ourselves that the average field does not broaden the lines. We then evaluate the effect of the dopant statistical distribution in the doping plane. Considering a given QD, we write the coulombic perturbation due to a single ionized impurity within the basis of the s and p states (we assume here for simplicity QDs with circular basis):

$$\begin{pmatrix} \lambda_{ss} & \lambda_{sp} \\ \lambda_{sp} & \lambda_{pp} \end{pmatrix}.$$

Both diagonal (λ_{ss} and λ_{pp}) and non-diagonal (λ_{sp}) couplings appear, which depend on the actual impurity in-plane position R ($R = 0$ corresponds to the center of the QD) and thus may lead to a broadening of the s-p energy transition. We have obtained that λ_{sp} leads to a maximum correction for the s-p transition energy of less than 1 meV, which is significantly smaller than the measured line-widths (3 to 10 meV; see Fig. 1). The diagonal correction $\lambda_{ss} - \lambda_{pp}$ can be more important, depending on the impurity position. However, we have checked that in our samples only the impurities located within $R < R_c = 6\,\mathrm{nm}$ can lead to a contribution larger than 1 meV. For instance in sample A1 (dopant concentration $N_s = 3.5\times10^{10}\,\mathrm{cm}^{-2}$) there is $\pi R_c^2\ N_s < 5\,\%$. Thus, as a general trend in our samples, the impurities are on the average too far from the dot region, so that the line broadening due to the statistical distribution in the doping plane cannot explain the experimental observations. Finally note that this contribution would lead to a broadening which is linear with N_s (in our low doping concentration case), in contradiction with our experiments.

We thus assume that the dominant broadening comes from fluctuations in the QD size. The QDs are modelled by truncated cones of height h, basis angle 30° and an average basis radius $\rho = \sqrt{ab}$. In order to account for the broadening of the FIR resonance as well as of the PL peak, we have to consider both fluctuations in the height h and in the radius ρ of the QDs.

As it is not clear if there is any growth-related correlation between h and ρ, we determine the fluctuations in vertical and lateral sizes from the experimental results obtained on the samples with the lowest doping level: A1 for series An and B1 for series Bn. In these samples the FIR magneto absorption resonances are associated with intraband $s-p$ transitions while the PL peak corresponds

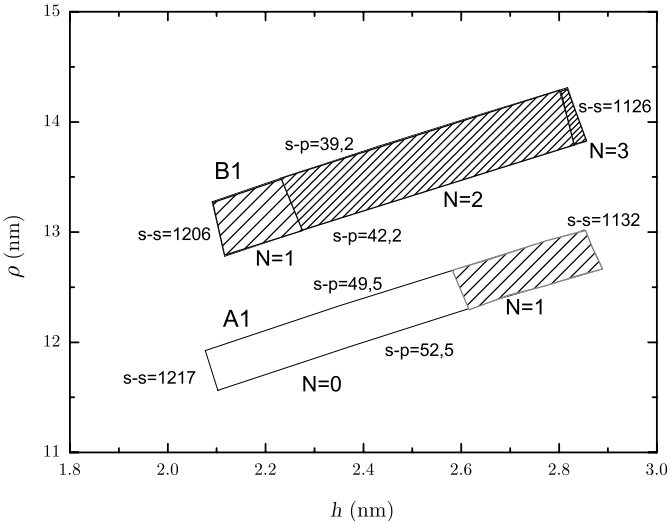

Fig. 6. Vertical (h) and lateral (ρ) size domain for QDs in samples A1 and B1 represented in a (h, ρ) diagram. Such domains are determined from the experimental results as explained in the text. s-p and s-s denote the energy of the intraband and interband transitions respectively and the solid lines correspond to constant s-p or s-s energy given in meV. The QD electron filling N calculated at zero magnetic field is indicated within the size domain.

to the interband $s-s$ transition. For each set of parameters (h, ρ), we calculate the intraband energy denoted $s-p$ as well as the interband energy denoted $s-s$ (energy of the ground trion state) and we draw in a ρ, h diagram the iso-energy lines corresponding to constant values of either $s-p$ or $s-s$. We then use the line-width of the FIR resonance and of the PL peak in order to obtain the size domain of the QDs for both An and Bn series, as follows.

Results obtained for A1 and B1 are shown in Figure 6. For A1 the PL peak spreads from 1132 to 1217 meV (these values correspond to the FWHM). The upper FIR intraband transition at $B = 0$ occurs at 51 meV with a FWHM of 3 meV. Thus, the two iso-energy lines $sp = 49.5$ and 52.5 meV together with the two iso-energy lines $ss = 1132$ meV and 1217 meV form a polygon which defines the vertical and lateral size domain for QDs of samples An. Each point within this polygon corresponds to a couple (h, ρ) which is consistent with the line-width of both PL and FIR resonance in A1. The QD size-distribution in series An is defined as follows: we consider the product of two Gaussian functions along the $s-s$ and $s-p$ iso-energy directions. The width of each Gaussian function is given by the sides of the polygon shown in Figure 6. A similar analysis using the experimental results in sample B1 give the QD size-distribution in series Bn. Note that our analysis leads to height fluctuations of $\sim \pm 0.4$ nm which correspond to variations of $\pm$one or two monolayers. The fluctuations in the average QD radius ρ are found to be $\sim \pm 1$ nm.

The size fluctuations correspond to QD energy level variations which can be larger than the Coulomb repulsion. For instance, let's consider two different QDs whose

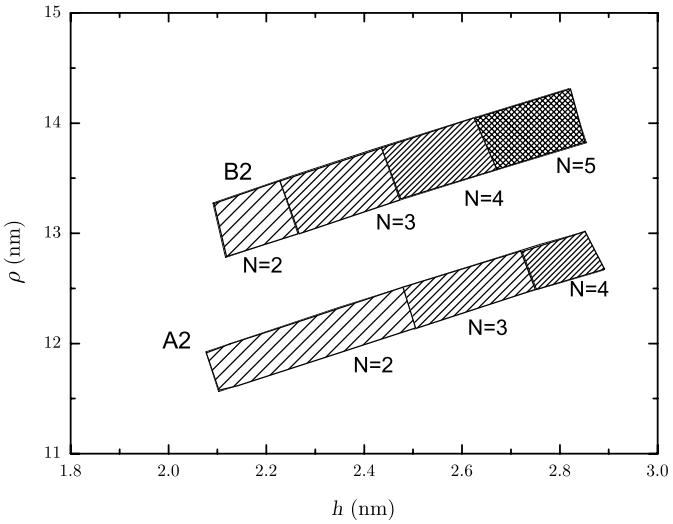

Fig. 7. Size domain and QD electron filling in samples A2 and B2 at zero magnetic field.

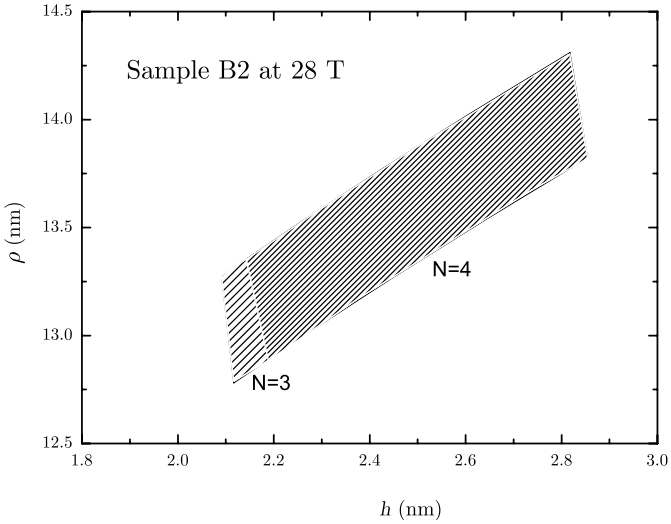

Fig. 8. QD electron filling in B2 in the (h, ρ) diagram at 28 T.

parameters (ρ, h) and (ρ', h') are within the polygon. If $\mu_{N+1}(\rho', h') = \mu_N(\rho, h)$, then both filling N and $N+1$ coexist in the sample. This leads to a non-uniform electron filling of the QD ensemble if one assumes a constant chemical potential at thermal equilibrium. The calculated resulting filling N is indicated for A1 and B1 in Figure 6. Two different fillings are obtained for A1. QDs with $N = 0$ do not contribute to the FIR intraband transition but only to the PL peak. Most of the populated QDs have a filling $N = 1$, higher filling appearing only in the tail of the Gaussian distribution. A similar analysis is shown in Figure 7 for sample A2 for which QDs with $N = 2, 3$ and 4 are predicted. The arrows labelled $N = 1, 2, 3, 4$ in Figure 1 indicate the calculated energy of the FIR transitions at $B = 8$ and 15 teslas for electron filling N. For each N, the values of h and ρ used in this calculation are the average (within the N-related part of the polygon) QD height and radius given by the size distribution of the series An. The agreement between the predicted transition positions and the experimental resonance is quite good for all the samples we have investigated. Note that we have analyzed in Figure 1 only the upper energy minimum which is associated to the B-increasing transitions in each sample. The lower energy resonance is associated to the B-decreasing transitions and occur at an energy close to that of the LO-phonon (~ 35 meV in the InAs/GaAs system). As a consequence, the polaron corrections, which we have neglect in the present calculations, become significant for these transitions, leading to a more intricate situation.

Finally, the lineshape of the upper energy resonance can be simulated for each sample by using the QD size-distribution, the different fillings N and the value of the electric dipole matrix element of the intraband transitions. In order to take into account all the other contributions to the broadening (for instance, the effect of the statistical distribution of the ionized dopants discussed above), a Gaussian energy-broadening of the various transitions with variance $\sigma = 1.5$ meV is included in the simulation. The dotted lines in Figure 1 show the simulated magneto-transmission spectra obtained for series An. They reproduce rather well both the intensity and the lineshape of the experimental resonances. For sample A1, only QDs with $N = 1$ participate significantly in the FIR absorption. As shown in Figure 6 by the hatched area, the size dispersion of these QDs is relatively small which explains the sharp resonance in this sample. On the contrary, several contributions ($N = 2, 3, 4$) occur in sample A2 which are not resolved but lead to a broadening of ~ 10 meV.

We now discuss the FIR results obtained on samples labelled Bn. Firstly same considerations as before permit to account for the line profiles of B1 and B2 samples in Figure 2 (not shown). Sample B1 is predicted to present a rather uniform filling $N = 2$ as it is shown in Figure 6. This occurs because $N = 2$ corresponds to the filling of the s shell and, as a consequence, there is a ~ 50 meV gap at $B = 0$ between μ_2 and μ_3 (see Fig. 5f). The size fluctuations are not important enough to exceed that energy. On the other hand, sample B2 is predicted to have a non-uniform filling (Fig. 7) at $B = 0$ with $N = 2$ to 5 and a remarkable homogeneous filling $N = 4$ at $B = 28$ T (Fig. 8). This arises because of the orbital Zeeman effect of the p states. A large gap opens at high magnetic field between μ_4 and μ_5 (~ 70 meV at 28 T, see Fig. 5f) which homogenize the filling of the QDs. The solid and bold dashed lines in Figure 3 show the theoretical B-dispersion of the magneto-optical transitions calculated for $N = 2$ and 4 respectively using $h = 2.5$ nm, $a = 13.2$ nm, $b = 14$ nm. Note that a fair agreement is obtained with the experimental results. In particular, such calculations explain the existence of a low energy resonance at 28 teslas around 20 meV in B1 which is not observed in B2 (Fig. 2). As mentioned in Section 3, sample B3 displays a broad and intense minimum which does not correspond to a QD excitation but behaves as the cyclotron resonance (CR) of a 2DEG. This observation suggests that all the electrons are no longer confined in the QDs but that some are delocalized in the wetting layer. The dashed line in Figure 3, which accounts

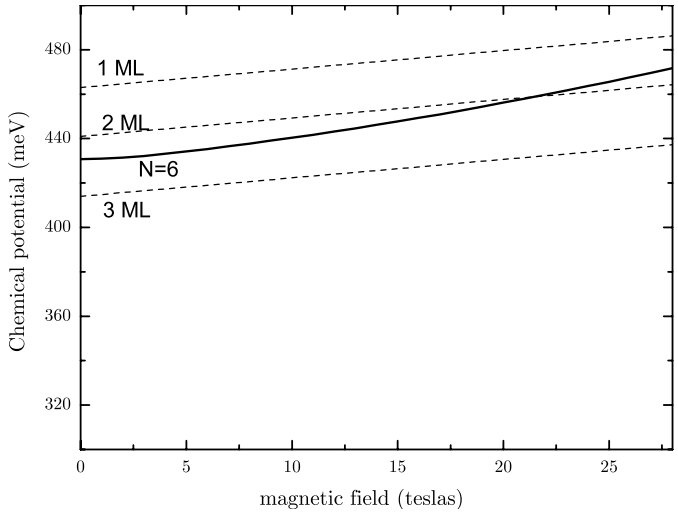

Fig. 9. Solid line: calculated QD chemical potential for $N = 6$ using the average QD size of sample B3. Dashed lines: wetting layer energy for WL thickness of 1, 2 and 3 ML.

very well for the experimental data, is the calculated CR energy using $m^* = 0.06m_0$. Such a cyclotron mass is quite reasonable for the In(Ga)As wetting layer. Indeed, taking into account the effects of strain, interdiffusion and band nonparabolicity due to the carrier confinement, brings the mass of In(Ga)As not far from that of GaAs. The situation in B3 can be understood as follows: QDs with $N = 5$ or 6 electrons are predicted to have a ground configuration which is bound but very near the WL continuum. This is illustrated in Figure 9 which shows the calculated chemical potential μ_6 in sample B3 using the average QD size of series Bn as well as the energy of the WL continuum for a thickness of 1, 2 and 3 mono layers. This means that for $N = 5$ or 6, the excited states are resonances inside the two-dimensional continuum of states of the WL. The FIR transitions between bound and continuum states correspond to weak and broad absorption which are not measured in our experiments. On the other hand, it is clear in Figure 9 that the 6-times charged QDs become unstable in the presence of trapping levels in the WL. In fact, the decrease of the WL continuum edge due to a 1 ML fluctuation ($\sim$ 25 meV, see Fig. 9) is of the same order of magnitude as the repulsive coulombic coupling among the bound electrons ($\sim$ 20 meV). Thus the configuration where 1 electron leaves the dot to become trapped in a WL defect can become energetically more stable and this would explain the existence of the CR-like line in sample B3.

We finally discuss the approximations made in our theoretical calculations of the multi-electron states. A configuration interaction scheme including s and p states was used neglecting both the d-states and the WL. One can now easily understand why the d states are little relevant in our analysis. For dots with $N = 1$ or 2 electrons (for instance in sample A1), only the s shell is occupied and there is no additional p-to-d transitions. The only effect of adding the d states is to slightly modify the energy position of the s-to-p transitions. This would not lead to any relevant contribution to the measured broadenings. For dots with $N = 3$ or 4 electrons, the p shell starts being occupied and p-to-d transitions are expected to lead to additional descending (energy decreases with the magnetic field) transitions. However, all the previous discussions related to the broadening effects have concerned exclusively ascending (energy increases with the magnetic field) transitions, so that the d states are irrelevant for the analysis of these transitions. Finally, QDs with $N = 5$ or 6 have a ground configuration which is very near to the WL continuum and have no bound excited states. We have not observed the FIR transitions between bound and continuum states. We have also neglected in our calculations the WL states which could lead to some corrections to the transitions energies. However, these high energy states should be rather insensitive to small size fluctuations, and thus would lead to dot-independent corrections and not contribute to the line broadening.

6 Conclusion

We have studied doped self-assembled InAs/GaAs QDs with an average filling ranging from 0.6 to 6 electrons using both FIR magneto-absorption technique and PL measurements. We have investigated two series of samples. In each series the doping level was varied from sample to sample, all the other growth parameters being exactly similar. The FIR spectra show significant changes in the magnetic field dispersion and in the line-width of the observed resonances as the doping level is varied. In order to analyse these results, we have calculated the few-electron states of the QDs under magnetic field, from which we have deduced the energy and the oscillator strength of the FIR magneto-optical transitions. The energy positions of the observed resonances agree with our calculations. The resonance lineshape can be explained by the filling fluctuations of the QDs. Among the different effects which can be invoked to explain the non-uniformity of the filling, we have considered both the statistical distribution of the dopant and the QD size fluctuations. We have calculated that the perturbation of the QD levels by the ionized dopants leads, for the low density of dopants used in our samples, to small energy corrections which could not account for the observed line broadenings. We thus conclude that the size dispersion constitutes the dominant effect which governs the filling uniformity of the QDs. For each sample series, we have determined the amplitude of the fluctuations in vertical and lateral size from the experimental results obtained on the sample with the lowest doping level. The QD size-distribution is then deduced for each sample as well as the filling distribution. The FIR magneto-transmission spectra are finally simulated. The simulations reproduce rather well both the intensity and the lineshape of the experimental resonances. A consistent description of QD size-dispersion and filling fluctuations is obtained for all the investigated samples. Moreover, our results show that up to 6 electrons can be transferred into the QDs but configurations with $N = 6$ electrons become unstable with the delocalization of some electrons

in the WL. In conclusion, FIR magneto-optical technique appears to be an effective tool to obtain informations regarding the dot size homogeneity and the related electron filling uniformity in doped self-assembled QD system.

This paper is dedicated to the memory of Jan Zeman who passed away on August 2002. We are very grateful to G. Bastard, O. Verzelen and A. Vasanelli for stimulating and fruitful discussions. The Laboratoire de Physique de la Matière Condensée at the École Normale Supérieure (ENS) is Unité Mixte de Recherche CNRS - ENS - Universités Paris 6 et Paris 7 (UMR 8551). This work has been partly supported by a New Energy and Industrial Technology Development Organization grant (NEDO, Japan) and by a Europeean Community project (IST-1999-11311 (SQID)).

References

1. S. Hameau, Y. Guldner, O. Verzelen, R. Ferreira, G. Bastard, J. Zeman, A. Lemaître, J.M. Gérard, Phys. Rev. Lett. **83**, 4152 (1999)
2. O. Verzelen, R. Ferreira, G. Bastard, Phys. Rev. B **62**, R4809 (2000)
3. S. Hameau, J.N. Isaia, Y. Guldner, E. Deleporte, O. Verzelen, R. Ferreira, G. Bastard, J. Zeman, J.M. Gérard, Phys. Rev. B **65**, 085316 (2002)
4. S.W. Lee, K. Hirakawa, Y. Shimada, Appl. Phys. Lett. **75**, 1428 (1999)
5. E. Finkman, S. Maimon, V. Immer, G. Bahir, S.E. Schacham, F. Fossard, F.H. Julien, J. Brault, M. Gendry, Phys. Rev. B **63**, 045323 (2001)
6. S. Maimon, E. Finkman, G. Bahir, S.E. Schacham, J.M. Garcia, P.M. Petroff, Appl. Phys. Lett. **73**, 2003 (1998)
7. J. Phillips, Pallab Bhattacharya, S.W. Kennerly, D.W. Beekman, M. Dutta, IEEE J. Quantum Electronics **35**, 936 (1999)
8. A.D. Stiff-Roberts, S. Chakrabarti, S. Pradhan, B. Kochman, P. Bhattacharya, Appl. Phys. Lett. **80**, 3265 (2002)
9. D. Loss, D.P. DiVincenzo, Phys. Rev. A **57**, 120 (1998)
10. O. Krebs, S. Laurent, P. Voisin, J.M. Gérard, S. Cortez, R. Ferreira, G. Bastard, M. Senes, X. Marie, T. Amand, Phys. Rev. Lett. **89**, 207401 (2002)
11. M. Fricke, A. Lorke, J.P. Kotthaus, G. Medeiros-Ribeiro, P.M. Petroff, Europhys. Lett. **36**, 197 (1996)
12. A. Wojs, P. Hawrylak, Phys. Rev. B **53**, 10841 (1996)
13. H. Drexler, D. Leonard, W. Hansen, J.P. Kotthaus, P.M. Petroff, Phys. Rev. Lett. **73**, 2252 (1994)
14. J.M. Gérard, J.B. Génin, J. Lefebvre, J.M. Moison, N. Lebouché, F. Barthe, J. Crystal Growth **150**, 351 (1995)
15. J.M. Gérard, J.Y. Marzin, G. Zimmermann, A. Pouchet, O. Cabrol, D. Barrier, B. Jusserand, B. Sermage, Solid State Electronics **40**, 807 (1996)
16. B. Grandidier, Y.M. Niquet, B. Legrand, J.P. Nys, C. Priester, D. Stiévenard, J.M. Gérard, V. Thierry-Mieg, Phys. Rev. Lett. **85**, 1068 (2000)
17. R. Ferreira, G. Bastard, Appl. Phys. Lett. **74**, 2818 (1999)
18. R.J. Warburton, B.T. Miller, C.S. Dürr, C. Bödefeld, K. Karrai, J.P. Kotthaus, G. Medeiros-Ribeiro, P.M. Petroff, S. Huant, Phys. Rev. B **58**, 16221 (1998)